

Multi-Echo Segmented k-space Imaging: An Optimized Hybrid Sequence for Ultrafast Cardiac Imaging

Scott B. Reeder,¹ Ergin Atalar,² Anthony Z. Faranesh,¹ and Elliot R. McVeigh^{1,2*}

Cardiac magnetic resonance imaging requires high temporal resolution to resolve motion and contrast uptake with low total scan times to avoid breathing artifacts. While spoiled gradient echo (SPGR) imaging is robust and reproducible, it is relatively inefficient and requires long breath-holds to acquire high time resolution movies of the heart. Echo planar imaging (EPI) is highly efficient with excellent signal-to-noise ratio (SNR) behavior; however, it is particularly difficult to use in the heart because of its sensitivity to chemical shift, susceptibility, and motion. EPI may also require reference scans, which are used to measure hardware delays and phase offsets that cause ghosting artifacts; these reference scans are more difficult and less reliable in the heart. Consequently, a hybrid EPI/SPGR sequence is proposed for application to rapid cardiac imaging. A detailed optimization of SNR and echo train length for multi-echo sequences is presented. It is shown that significant reductions in total scan time are possible while maintaining good image quality. This will allow complete motion sampling of the entire heart in one to three breath-holds, necessary for MR cardiac dobutamine stress testing. Improved speed performance also permits sampling of three to six slices every heartbeat for bolus injection perfusion studies. *Magn Reson Med* 41:375–385, 1999. © 1999 Wiley-Liss, Inc.

Key words: magnetic resonance (MR); cardiac imaging; fast imaging; echo planar imaging; gradient echo imaging; stress testing; perfusion

INTRODUCTION

In recent years, improvement in gradient hardware technology as well as in the ability of MR systems to manipulate and process raw data more rapidly has brought significant advances to cardiac MRI. While rapid imaging techniques are routinely used to capture motion of the heart, areas of active investigation in cardiac MRI require reductions in total scan time. Such applications include bolus tracking of contrast agents through the myocardium (1–5). Accurate characterization of perfusion defects requires sampling of three to six imaging planes with one to two heartbeat temporal resolution. Moreover, real-time MR “fluoroscopy” (6, 7) requires refresh rates of 5–20 frames/sec, while cardiac MR dobutamine stress testing requires the acquisition and reconstruction of complete cardiac movie loops within one to five heartbeats.

Segmented spoiled gradient echo (SPGR) breath-hold imaging is a well-established method that is very suitable

for imaging the heart. It is a robust technique with excellent reproducibility, adequate signal-to-noise ratio (SNR), and insensitivity to motion and off-resonance effects caused by susceptibility and chemical shift. While it is sufficiently rapid for capturing motion of the heart, only a single movie of one imaging plane is usually acquired within one 15- to 20-sec breath-hold. This is largely caused by the low efficiency of an SPGR sequence, resulting from the high overhead of one RF excitation for each k_y line sampled.

Multi-echo imaging techniques, such as echo planar imaging (EPI) (8), fast spin echo (FSE) (9), and gradient and spin echo (GRASE) (10), have good SNR behavior and very low imaging times, capable of acquiring entire images in 40–300 msec. EPI, for example, would permit acquisition of cardiac movie frames with high temporal resolution in one to two heartbeats. As described by McKinnon, when EPI is applied to the heart for cine acquisitions, sequential excitation/sampling of slices is performed fundamentally the same way as segmented SPGR acquisitions (11). This implies that the magnetization behavior of cardiac EPI and SPGR is very similar and can be analyzed on a continuum of echo train lengths. SNR gains with EPI are achieved mainly through improvements in sequence efficiency (12) and, as described later, through increased T_1 recovery as the echo train length increases. EPI also has the added advantage of superior tag/myocardial contrast (13).

While single-shot cardiac EPI suffers from severe distortion, resulting from the inhomogeneous magnetic field in the mediastinum, multishot, or interleaved, EPI has been successfully applied to cardiac imaging by McKinnon et al. (11). Interleaving reduces distortion in regions of high-field inhomogeneity, although most four- to eight-shot EPI images still suffer from significant distortion and T_2^* signal loss, particularly in regions adjacent to large coronary veins, where susceptibility gradients are especially high (14).

In this work, we develop an ultrafast multi-echo cardiac SPGR tagging sequence, by taking the approach of moving from SPGR imaging toward EPI. By increasing the number of echoes acquired after each radio frequency (RF) excitation, significant fractional increases in the efficiency of the pulse sequence and decreases in total scan time are achieved. Pulse sequence dead periods are reduced to the minimum times possible using hardware-optimized trapezoid (HOT) gradient pulses (15). Expressions that describe the echo train length that optimizes SNR, based on myocardial T_2^* are derived. Criteria for setting upper bounds on echo train length to reduce distortion caused by field inhomogeneities are also presented. This analysis can be extended for imaging applications in any region of the body.

¹Department of Biomedical Engineering, Johns Hopkins University School of Medicine, Baltimore, Maryland.

²Department of Radiology, Johns Hopkins School of Medicine, Baltimore, Maryland.

*Correspondence to: Elliot R. McVeigh, Ph.D., Department of Biomedical Engineering, 407 Traylor Building, 720 Rutland Avenue, Johns Hopkins University School of Medicine, Baltimore, MD 21205.
E-mail: emcveigh@mri.jhu.edu

Received 1 August 1997; revised 20 July 1998; accepted 22 July 1998.

THEORY

Echo Train Length and SNR Optimization

Optimization of SNR for short TE, single-echo SPGR imaging previously has been shown to be independent of TR at steady state for constant scan time and bandwidth (12). As dead time is added to the TR, the increase in signal from T_1 recovery is exactly balanced by decreases in sequence efficiency.

Increasing the echo train length of a multi-echo sequence, however, increases not only TR, allowing more time for T_1 recovery, but also sequence efficiency, further increasing signal. As the echo train length becomes large, incremental increases in efficiency are low and T_2^* decay begins to dominate the growing T_1 recovery. An intermediate optimal echo train length is expected to exist and is derived later herein.

We have previously reported (12) that the SNR of any imaging sequence is

$$SNR \propto S \Delta V \sqrt{\eta} \sqrt{T_s} \quad [1]$$

where S is the relative signal of the sequence, ΔV is the voxel volume, η is the sequence efficiency, and T_s is the total scan time. For a multi-echo imaging sequence, with n echoes in the echo train (16), the efficiency is

$$\eta = \frac{nN_x T}{T_d + nT_{ro}} \quad [2]$$

where $N_x T$ is the sampling window for an echo; T_d is the time for slice selection, phase-encoding prephasing, and readout prephasing; and T_{ro} is the time between echoes. For large n , η is relatively independent of n , and the SNR can be maximized by optimizing the relative signal, S , given as

$$S(m) = M_o \left((\cos \alpha e^{-TR/T_1})^m + (1 - e^{-TR/T_1}) \frac{1 - (\cos \alpha e^{-TR/T_1})^m}{1 - \cos \alpha e^{-TR/T_1}} \right) \sin \alpha e^{-TE/T_2^*} \quad [3]$$

where α is the tip angle and m is the RF pulse number. As m becomes large, the signal approaches steady state:

$$S = \frac{M_o(1 - e^{-TR/T_1}) \sin \alpha e^{-TE/T_2^*}}{1 - \cos \alpha e^{-TR/T_1}} \quad [4]$$

Assuming the Ernst angle is used, then

$$\cos \alpha = e^{-TR/T_1} \quad [5]$$

and

$$\sin \alpha = \sqrt{1 - e^{-2TR/T_1}} \quad [6]$$

so that

$$S = \frac{M_o(1 - e^{-TR/T_1}) e^{-TE/T_2^*}}{\sqrt{1 - e^{-TR/T_1}}} \quad [7]$$

For a multi-echo sequence, let $TR = T_d + nT_{ro}$, and $TE \approx T_d + \zeta nT_{ro}$, and $\zeta \in (0, 1)$ determines the position in the echo train where SNR is to be optimized. Inserting expressions for TR and TE into 7,

$$S = \frac{M_o(1 - e^{-T_d/T_1} e^{-nT_{ro}/T_1}) e^{-T_d/T_2^*} e^{-\zeta nT_{ro}/T_2^*}}{\sqrt{1 - e^{-2T_d/T_1} e^{-2nT_{ro}/T_1}}} \quad [8]$$

The optimum echo train length is determined by differentiating Eq. 8 with respect to the echo train length, n , and setting the result to zero. As shown in Appendix A, the optimal echo train length is

$$n_{opt} \approx \frac{T_2^*}{2\zeta T_{ro}} \quad [9]$$

This simple expression gives the optimal echo train length of a gradient echo EPI echo train, required to maximize image SNR at the $(\zeta n_{opt})^{th}$ echo, for constant scan time and steady-state imaging. Note that this expression is independent of T_1 and TR .

For many applications ζ will be chosen as 0.5. In this case, Eq. 9 can be rearranged to describe the optimal readout sampling time of the echo train as

$$T_{smp} = n_{opt} T_{ro} \approx T_2^* \quad [10]$$

showing that optimal duration of the echo train is approximately T_2^* . The readout sampling time that maximizes SNR for steady-state imaging is easily determined if the T_2^* of the tissue is known.

This result can be interpreted as follows. As the echo train length increases, TR increases, increasing T_1 recovery between RF pulses. As the echo train length increases, however, the effective TE also increases; eventually, T_2^* dominates the signal such that further increases in echo train length decrease signal. Efficiency has a small effect, since efficiency is relatively independent of echo train length for large echo train lengths.

The T_2^* in the hearts of normal volunteers has been measured at 1.5 T (14). It was found that the T_2^* ranged from 26 to 41 msec in the septal, lateral, posterior, and anterior walls. In focal regions near the posterior vein of the left ventricle, however, T_2^* was found to be 12 msec. This value was measured in 8-mm slices, although no dependence on T_2^* with slice thickness was observed in this study. According to the cited analysis, with $T_2^* = 12$ msec, the total sampling time during readout should be approximately 12 msec, to maximize SNR in these regions. With $T_{ro} = 1.3$ msec, no more than nine echoes should be used in the readout echo train.

For some applications, the amplitude of the first echo should be maximized. In this case, ζ will be small, and the optimal echo train length based on this analysis will be high. Degradation of spatial resolution becomes the limiting factor, however, because T_2^* decay will diminish spatial resolution in the phase-encoding direction for echo trains of long duration (17).

The steady-state assumption may not be valid for many applications, particularly gated cardiac applications with relatively few RF pulses within a cardiac cycle as well as multislice applications. As an extreme example, an imaging sequence that uses one RF excitation ($m = 1$ in Eq. 3) and waits for full T_1 recovery before the next excitation would maximize SNR by using the shortest possible echo train length to minimize T_2^* decay. This scenario assumes that other slices can be imaged during this recovery period. As the number of consecutive RF pulses increases, the optimal readout sampling time will increase from the minimum possible toward T_2^* at steady state. Characterization of the transition point and the SNR behavior may be important for many applications.

The behavior of the SNR as echo train duration increases for different numbers of RF pulses in the approach to steady state is plotted in Fig. 1. For these calculations, T_2^* and T_1 were set to 30 msec and 800 msec, respectively. The initial dead time (T_d) was 2 msec, the plateau time of the readout gradient was 1 msec, and the total time between echoes (T_{ro}) was 1.3 msec. The flip angle that maximizes SNR at the m^{th} RF pulse was calculated and used for each curve. Dead times were accounted for by multiplying the

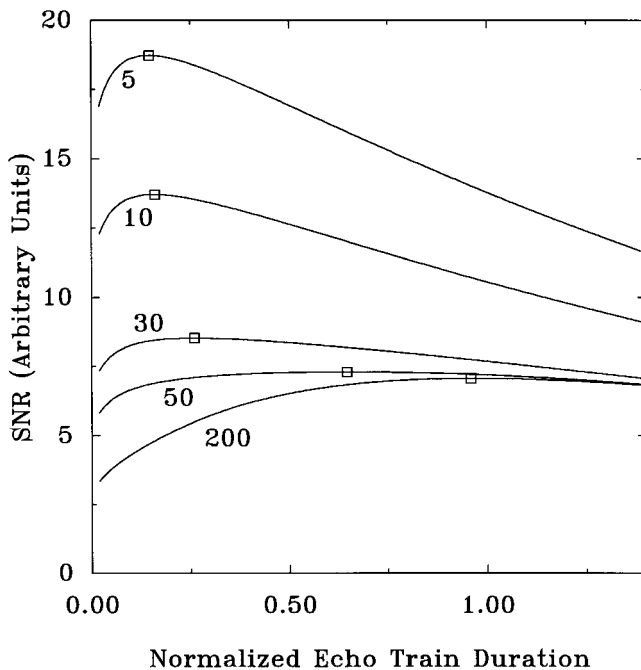


FIG. 1. Theoretical SNR for constant scan time, plotted against echo train duration, after 5, 10, 30, 50, and 200 RF excitations. The echo train duration has been normalized by T_2^* , which was set to 30 msec for this simulation. SNR is calculated after the last RF excitation in the middle of the echo train ($\zeta = 0.5$). Other imaging parameters include $T_d = 2$ msec, $N_x = 256$, $BW = \pm 64$ kHz, and $T_1 = 800$ msec. Squares are plotted at the maxima of each curve.

relative signal with the square root of efficiency (Eq. 1). It has been assumed that full T_1 recovery has been allowed after each approach to steady state; other slices are imaged during this recovery period. The echo train duration in Fig. 1 has been normalized by T_2^* , to emphasize that the optimum echo train duration is approximately T_2^* as steady state is reached.

There are three regions of signal behavior in these curves. For low echo train lengths, increases in SNR result from improvements in efficiency, as well as increased T_1 recovery, as the echo train length increases. As echo train lengths become greater than approximately four to five echoes, efficiency improves marginally and contributes little to further improvements in SNR. As the readout duration increases, SNR continues to increase through improved T_1 recovery; however, T_2^* decay begins to dominate, and SNR decreases with increases in echo train length.

Several inferences can be drawn from this figure. First, SNR varies smoothly with echo train length. At steady state, the maximum SNR occurs at 30 msec, equal to T_2^* used in the simulation and agreeing with Eq. 10. Although a sharp transition in the optimal echo train length takes place as the number of RF pulses increases toward steady state, the actual SNR is relatively insensitive to the echo train length near the optimum.

Figure 2a plots the optimal echo train duration against RF pulse number for $T_2^* = 10$ msec, 30 msec, and 50 msec. Figure 2b plots the SNR at the optimal echo train duration against RF pulse number. The dashed lines in this figure represent the maximum SNR if the echo train duration is set to T_2^* for all cases.

These figures show that the optimal echo train duration is never more than T_2^* , increasing toward T_2^* as the echo train duration increases. It is interesting to note that the transition “elbow” moves farther to the right as the T_2^* decreases. Substantial increases in SNR are realized for acquisitions with low numbers of RF excitations, as would be expected for multislice imaging. Fixing the echo train duration at T_2^* makes significant decreases in SNR when only low numbers of RF pulses are used.

As an example, consider a cardiac imaging sequence that uses 50 RF pulses during a heartbeat. The optimum echo train duration in this case would be approximately 22 msec (Fig. 2a, assuming $T_2^* = 30$ msec). Figure 2b shows that the maximum SNR (arbitrary units) obtained under these conditions would be approximately 7. The dashed line in this figure indicates that a sequence with an echo train duration of 30 msec ($= T_2^*$) would have negligibly lower SNR than the optimal echo train duration of 22 msec.

An important caveat must be considered when interpreting these results. Specifically, boundary conditions may apply for particular applications. For example, in breath-hold cardiac imaging, the total imaging time is generally less than 15–20 sec, and the time resolution of a movie frame is usually 20–50 msec. In this case, it would not be practical to design a multislice acquisition with a single echo per image per heartbeat. Longer echo trains, or more RF pulses, would be needed to acquire the entire data matrix within the breath-hold period. Since the reduction

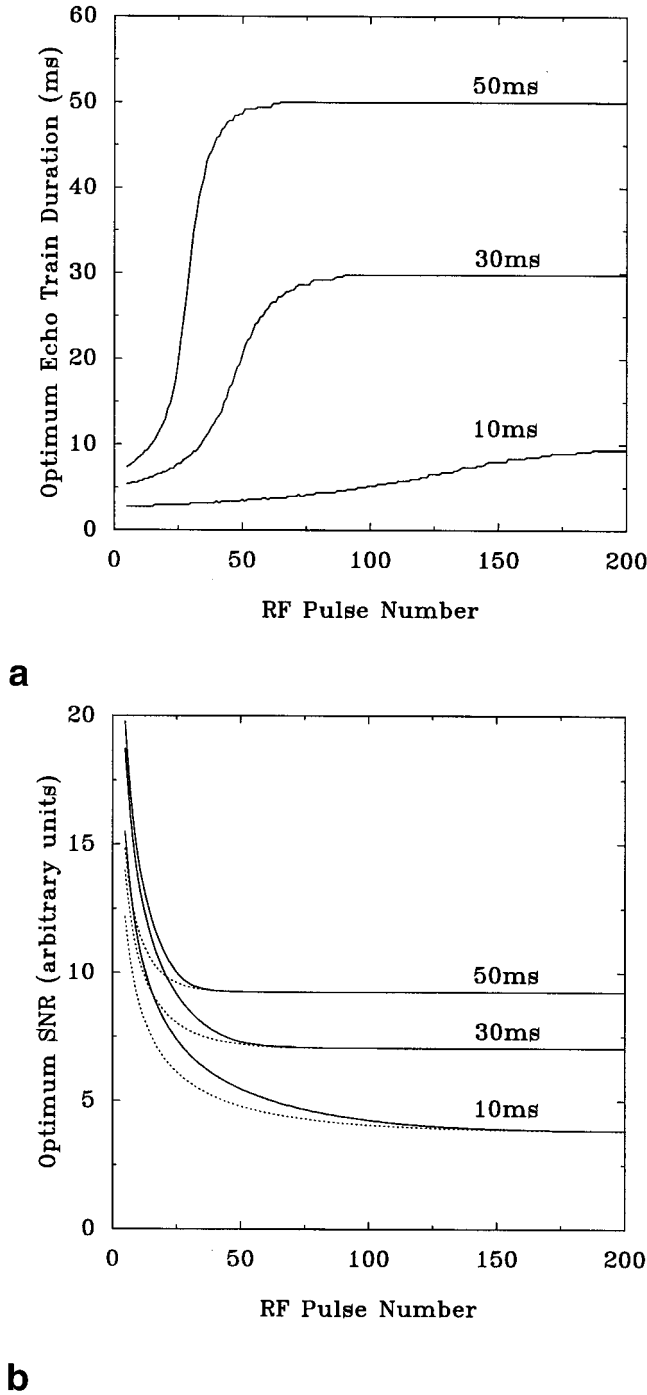


FIG. 2. **a**: Optimal echo train length plotted against RF pulse number in the approach to steady state for $T_2^* = 10$ msec, 30 msec, and 50 msec. **b**: SNR calculated at the optimal echo train length plotted against SNR for the same parameters as (a). The dashed lines are the maximum SNR if the echo train duration equals T_2^* . Other parameters include $T_1 = 800$ msec, $T_d = 2$ msec, $T_{ro} = 1.3$ msec, and 1-ms readout sampling time.

in SNR for low numbers of RF pulses is not substantial, as seen with the dashed lines in Fig. 2, setting the echo train duration equal to the T_2^* may be close to optimum for many cases.

Field Inhomogeneities: Reducing Distortion

Chemical shift, susceptibility, and field inhomogeneities are spatially dependent inhomogeneities that can be highly irregular and sample dependent. These can be described by changes in the static field, $\Delta B(x, y)$, and an off-resonance chemical shift, f (Hz). The spins in an object accrue additional phase from these off-resonance effects, and distortion in the phase-encoding direction will result. As shown in Appendix B, this distortion (in pixels) can be written

$$\Delta y' = \frac{\gamma}{2\pi} (\Delta B(x, y) + f/\gamma) T_{\text{samp}} \quad [11]$$

where T_{samp} is the readout sampling time during which the phase of off-resonance spins evolve, causing distortion. The sampling time is the product of the echo train length, n , and the duration of a complete readout trapezoid in an echo train, T_{ro} . Reduction of distortion can be achieved either through reduction of the echo train length or the time between echoes.

Recent measurements show the average peak-to-peak field inhomogeneities to be 71 ± 14 Hz over various regions of the human heart ($n = 5$) at 1.5 T (14). With $\gamma/2\pi \Delta B(x, y) = 71$ Hz, $f = 0$, $n = 32$, and $T_{ro} = 1.3$ msec ($T_{\text{samp}} = 42$ msec), the distortion will be three pixels in the phase-encoding direction, as calculated by Eq. 11. For applications that require accurate quantification of cardiac motion (18), this is a large distortion.

For particular applications, criteria for acceptable distortion may be different. In general, for a maximum acceptable shift of $\Delta y'_{\text{max}}$, the maximum number of echoes is

$$n_{\text{max}} = \frac{\Delta y'_{\text{max}}}{\gamma/2\pi \Delta B_{\text{max}} T_{ro}} \quad [12]$$

As an example, the maximum acceptable shift for myocardial motion tracking applications might be 0.5 pixels. With $\gamma/2\pi \Delta B_{\text{max}} = 71$ Hz and $T_{ro} = 1.3$ msec, the maximum number of echoes is between three and five. This suggests that a low number of echoes should be used for echo planar imaging of the heart. Higher sampling bandwidths would increase echo train lengths while maintaining the same readout sampling time.

Additional Echo Train Length Considerations

Reduction of signal loss in regions of short T_2^* and minimization of image distortion require that the cardiac imaging sequence use low echo train lengths. Several additional factors must be considered for determination of the optimal echo train length. Overall acquisition time, SNR, and image quality can be greatly affected by the proper choice of parameters.

Sequence Efficiency and Echo Time Shifting.

As described in Echo Train Length and SNR Optimization, SNR is proportional to the square root of efficiency for constant scan time. In general, increasing the echo train length improves efficiency and therefore SNR. This higher

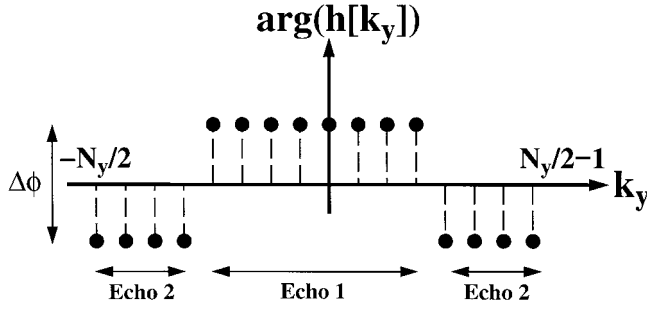


FIG. 3. Potential phase modulation of a two-echo data set with centric phase encoding. Here, $N_y = 24$, and the phase difference between the first and second echoes is ϕ . Such discontinuities can result from off-resonance effects and chemical shift as well as hardware phase shifts and time delays.

sequence efficiency is a primary advantage of EPI over SPGR imaging.

Ghosting artifacts present serious difficulties for EPI, especially in the presence of field inhomogeneities and T_2^* decay. One solution to alleviate ghosting artifacts from both phase and amplitude discontinuities is to slide the echo train at incrementally increasing delays after the RF excitation. This technique, known as echo time shifting (ETS) (19), is highly effective for creating smooth phase and amplitude transitions across k -space in the phase-encoding direction and is a standard feature of most EPI sequences. Implementation of ETS requires additional dead time, however, approximately equal to the time required to play one complete readout trapezoid in a readout train (T_{ro}). For sequences with short echo trains, the additional dead time required for ETS significantly reduces the increase in efficiency obtained by adding echoes to the single-echo SPGR sequence, which does not require ETS.

Ghosting with Small Echo Train Lengths.

The ghosting point-spread function (PSF) for amplitude and phase discontinuities, as well as filter time delays, has been described (20). In this work it was shown that the artifacts that arise from phase or amplitude discontinuities cause blurring, rather than ghosting, for an echo train length of two. For example, consider a phase discontinuity for the centric phase encoding ordering scheme depicted in Fig. 3 for two echoes, with a phase discontinuity, $\Delta\phi$, between even and odd echoes. The PSF in the phase-encoding direction with this discontinuity (20) is

$$H_\phi[n_y] = N_y \cos \frac{\Delta\phi}{2} \delta[n_y] + 2j \sin \frac{\Delta\phi \sin \pi n_y/2}{2 \sin \pi n_y/N_y} e^{j\pi n_y/N_y} \sum_{k=-(N_y/2)+1}^{(N_y/2)-1} \delta[n_y - k], k \text{ odd} \quad [13]$$

where N_y is the number of phase-encoding steps.

Figure 4 plots the magnitude of the PSF calculated from Eq. 13 for $\Delta\phi = 0^\circ, 30^\circ$, and 90° . This figure shows that substantial phase discontinuities are required to degrade the spatial resolution of a two-echo readout, suggesting that sequences with only two echoes per RF excitation may not require ETS to smooth phase discontinuities. Furthermore, time delays and constant phase offsets from hardware inaccuracies may need less precise correction through reference scans and post-processing, usually performed for ghost artifact reduction (21).

Fractional Echoes

Acquisition of fractional echoes during readout are commonly used in SPGR imaging to reduce both TR and TE while preserving spatial resolution. Fractional echoes are particularly advantageous for tagging studies, since they facilitate rapid sampling of higher Fourier components of the tagging pattern, necessary for good tag tracking (18, 22). They are usually avoided in EPI, since the time between successive echoes is not constant and will produce ghosting or blurring artifacts, resulting from phase and amplitude discontinuities between successive k_y lines. A two-echo acquisition avoids this problem, since there is only one interecho interval.

MATERIALS AND METHODS

Pulse Sequence

A multi-echo SPGR pulse sequence was written for a GE Signa 1.5-T Horizon (version 5.6) and is shown in Fig. 5. This scanner has shielded gradients with a maximum gradient strength of 2.2 G/cm and a slew rate of 120 T/m s on all three axes. This sequence uses HOTs to achieve the

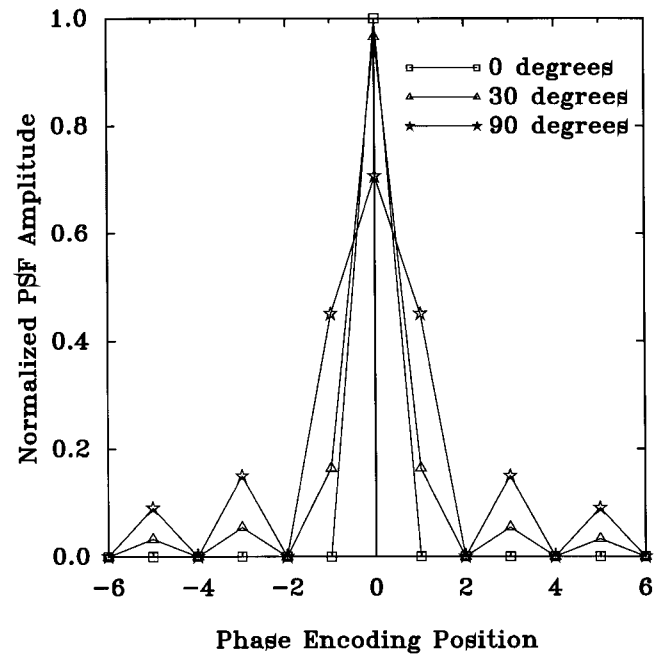


FIG. 4. Normalized PSF in the phase-encoding direction, resulting from constant phase offsets of $0^\circ, 30^\circ$, and 90° , for a centrically encoded two-echo sequence.

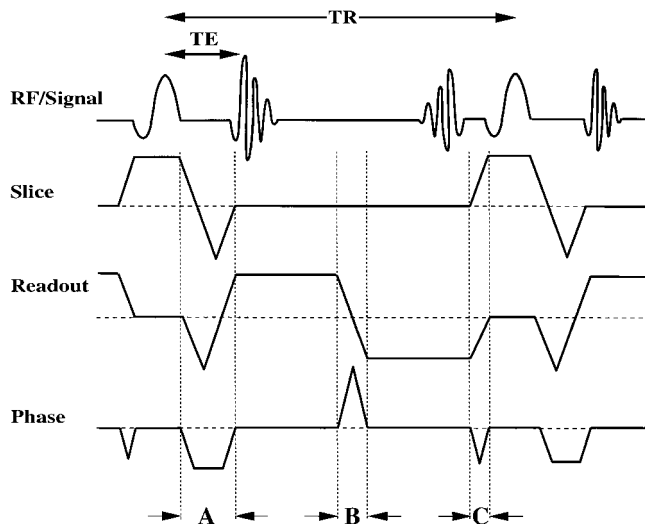


FIG. 5. Hybrid SPGR/EPI pulse sequence with HOT pulses during dead periods A, B, and C. Shown is an echo train length of two, with HOT pulses also during the phase-encoding blips, and fractional readouts. Echo time shifting (ETS) is not shown here.

minimum possible dead periods for a given oblique orientation (15). For HOT optimization, a dead period is defined as any set of gradient pulses that does not occur during RF excitation or readout acquisition. The only restriction on these waveforms during oblique rotation is that the starting and ending amplitudes, as well as the area of each dead period waveform, must be conserved; the shape of these waveforms during the dead period is not important, as long as hardware limitations are not exceeded. It should be noted that the duration of the dead periods, and hence TE and TR, will depend on the orientation of the imaging plane. For this work, HOT optimization was also applied to the phase-encoding blip region for multiple echo sequences.

The duration of the slice plateau can also be adjusted to minimize the sequence TR. In general, increasing the gradient strength of the slice selection gradient will decrease the total time required for slice selection. As the gradient strength is increased further, the ramp area of the slice selection trapezoid becomes large and must be compensated by the slice-refocusing lobe. An optimum slice-selection plateau duration will exist, as previously described (12). For the implementation of this sequence on our current scanner, however, the RF subsystem was unable to provide optimal duration RF pulses, and a longer slice selection plateau was used. This increased TR by approximately 350 μ s for typical imaging parameters.

Myocardial motion is visualized through the use of parallel DANTE/SPAMM tagging pulses (23, 24). Black-blood imaging is achieved through end-diastolic selective presaturation of atrial and ventricular blood basal and apical to the imaging slice, as well as an end-systolic selective inversion of atrial blood. This ensures that signal from blood flowing into the ventricles during diastole will be attenuated during the subsequent heartbeat (25).

The typical TR for this two-echo sequence is 4.6–4.8 msec, with 160 fractional echoes and a ± 64 kHz bandwidth. If 20 phase-encoding lines are acquired for each movie frame every heartbeat, time resolution for each time

frame will be 46–48 msec. The movie from one slice can be acquired in three heartbeats with 60 k_y lines per image using an asymmetric field of view (FOV) in the phase-encoding direction. This is adequate resolution for tracking of parallel tags perpendicular to the readout direction (18). Three 15-sec breath-holds would permit the collection of movies from 15 slices. Reduction of the FOV in the phase-encoding direction decreases the total scan time by reducing the number of phase-encoding steps without changing image resolution.

Acquisition of multiple slices within a breath-hold is advantageous for other applications, such as MR coronary angiography. This technique often relies on multiple breath-holds or navigator echo techniques (26). Increasing the number of slices acquired during a breath-hold reduces slice misregistration that can occur between slices acquired in different breath-holds (27). This will reduce the dependence on navigator echoes.

Special image reconstruction is not performed for this sequence for imaging with more than one echo per RF excitation. As described elsewhere (28), we have calibrated our scanner for time delays and tuned “compensation blips” to correct for these delays using gradient waveform. These delays are compensated for oblique imaging as well and remove the need for reference scans and post-processing algorithms. For low echo train lengths, however, precise tuning of timing delays is less essential, as discussed earlier.

RESULTS

Speed Performance with Multiple Echoes

Figure 6a plots the average time between echoes against echo train length, with and without ETS, for $N_x = 256$, $N_y = 120$, BW = ± 64 kHz, 0.8-cm slice thickness, and a 32-cm FOV, and for our gradient hardware parameters (2.2 G/cm maximum gradient strength and a 120 T/m s slew rate). The speed performance of one and two fractional echo acquisitions (160 points) is also shown. The optimal slice plateau duration has been used in these calculations. The effects of improving gradient hardware performance are seen in Fig. 6b, which plots the average time per echo against echo train length for the same parameters in 6a, except with a maximum gradient strength of 4 G/cm and a 200 T/m s slew rate. The effects of bandwidth on imaging speed are shown in Fig. 6c for the high-performance gradients (4 G/cm, 200 T/m s), and a ± 125 -kHz bandwidth.

From these figures it can be seen that echo time shifting seriously impairs speed performance of this sequence for short echo trains. It is also apparent that a two-echo readout with fractional echo has the best speed performance; this sequence can acquire data faster than even a 10-echo train length sequence with full echoes. Only marginal improvements in speed performance can be achieved with the faster gradient hardware. Substantial increases in speed are best attained with increases in bandwidth.

Efficiency Performance with Multiple Echoes

Figure 7a–c plots the sequence efficiency (as defined by Eq. 2) against echo train length for the identical parameters

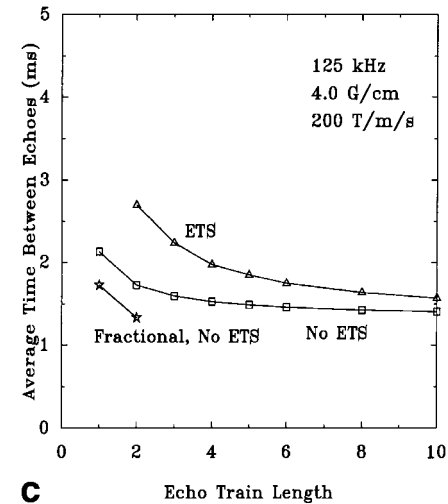
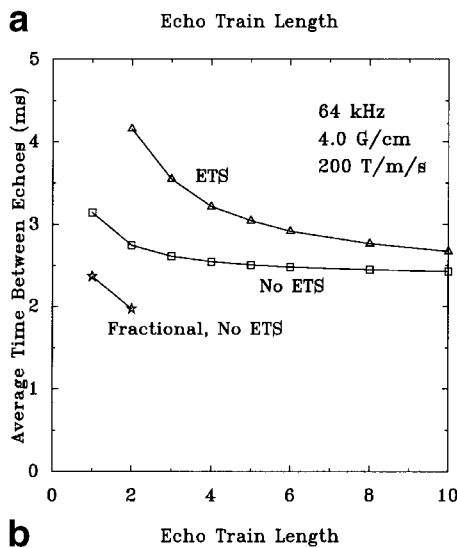
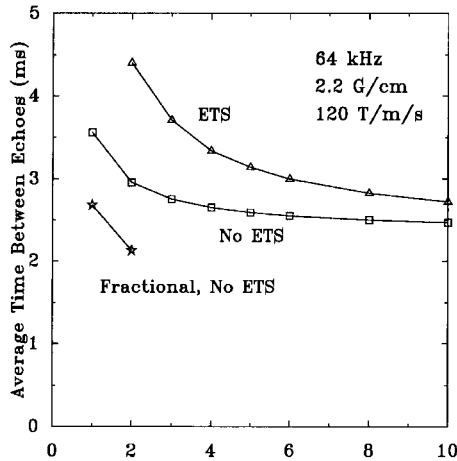


FIG. 6. Average acquisition time per echo plotted against the echo train length, with and without echo time shifting (ETS). For all cases shown, $N_x = 256$, $N_y = 120$, $\Delta z = 0.8$ cm, and FOV = 32 cm. For one- and two-echo sequences, fractional readouts (160 points) reduce the average time between echoes. **a:** BW = ± 64 kHz, $G_{\max} = 2.2$ G/cm, and slew rate = 120 T/m/s. **b:** BW = ± 64 kHz, 4.0 G/cm, 200 T/m/s slew rate. **c:** BW = ± 125 kHz, 4.0 G/cm, 200 T/m/s slew rate.

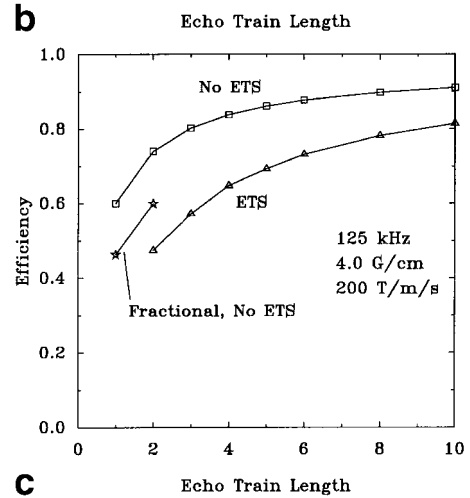
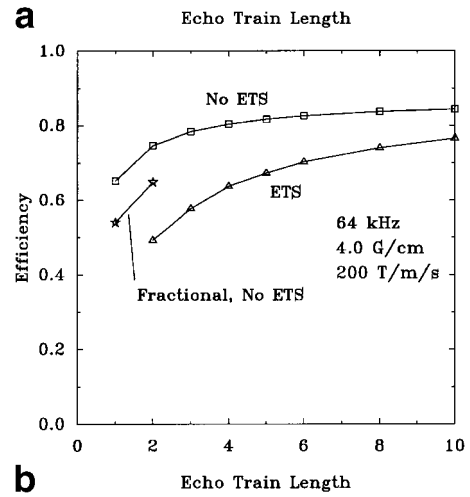
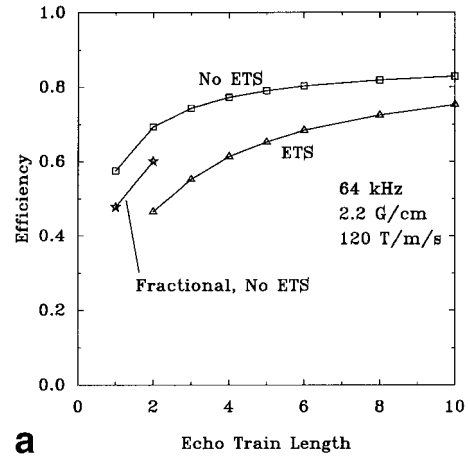


FIG. 7. Efficiency plotted against the echo train length, with and without ETS. For all cases shown, $N_x = 256$, $N_y = 120$, $\Delta z = 0.8$ cm, and FOV = 32 cm. For one- and two-echo sequences, fractional readouts (160 points) will reduce sequence efficiency. **a:** BW = ± 64 kHz, $G_{\max} = 2.2$ G/cm, and slew rate = 120 T/m/s. **b:** BW = ± 64 kHz, 4.0 G/cm, 200 T/m/s slew rate. **c:** BW = ± 125 kHz, 4.0 G/cm, 200 T/m/s slew rate.

shown in Fig. 6a–c. Substantial incremental increases in sequence efficiency can be achieved by increasing the echo train length. The greatest increases occur by adding one or two echoes to the single-echo sequence.

ETS decreases sequence efficiency, as do fractional echoes. The efficiency of the fractional two-echo acquisition, however, is higher than either the fractional or full

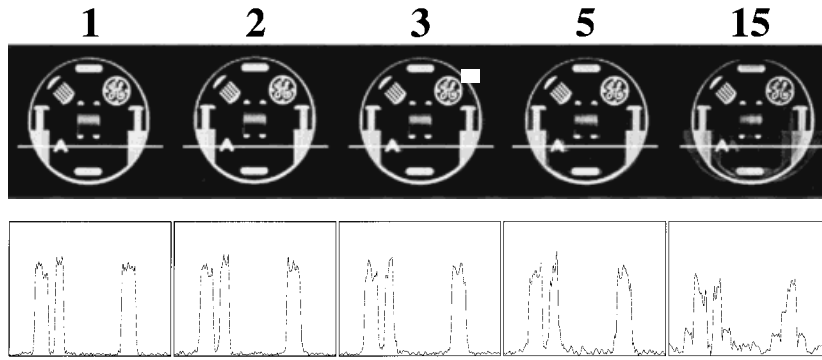


FIG. 8. Multi-echo SPGR images acquired with 1, 2, 3, 5, and 15 echoes in a Q/A phantom. Profiles along the white lines in the phase-encoding direction show minimal edge blurring for lower echo train lengths. Centric phase encoding has been used for one and two echo images and standard phase encoding for the three, five, and 15 echo images. ETS has not been used, and no post-processing corrections have been made while maintaining comparable image quality for low echo train lengths. Other imaging parameters include ± 64 kHz, BW, 256 \times 180 matrix size, 24-cm FOV, and 10° flip angle. TR was 4.2 msec, 6.7 msec, 9.3 msec, 13.9 msec, and 37.1 msec for the 1-, 2-, 3-, 5-, and 15-echo acquisitions.

single-echo acquisition. Increasing the bandwidth while improving the speed performance adversely affects SNR in two ways. First, increasing bandwidth directly decreases SNR, since $\text{SNR} \propto \sqrt{BW}$. Second, increases in bandwidth will decrease the sequence efficiency, further reducing SNR, since $\text{SNR} \propto \sqrt{\eta}$. Increasing the gradient strength and switching time will make marginal improvements in efficiency, and thus SNR, although high maximum gradient strengths are required for high bandwidth imaging at reduced FOVs.

Low Echo Train Length Images

Figure 8 shows axial images of a Q/A phantom, acquired with 1, 2, 3, 5, and 15 full echoes. No post-processing delay or phase corrections have been made. Profiles through the phantoms in the phase-encoding direction show some blurring as echo train length increases, although image quality is good, even for the five-echo acquisition, where some blurring is seen. Ghosting artifacts are seen for the 15-echo acquisition. The SNR was high in all phantom images, ranging from 54 to 83.

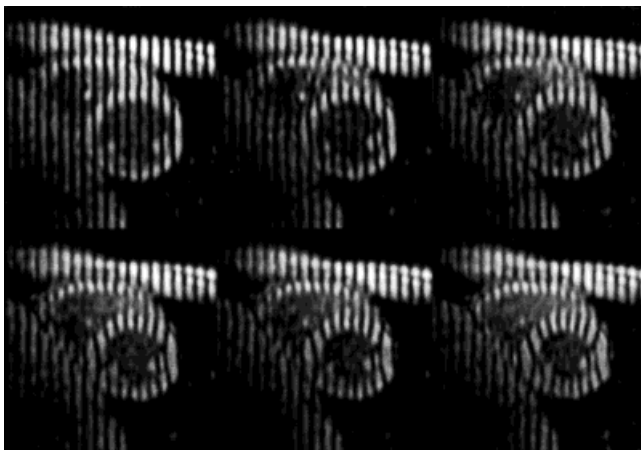


FIG. 9. Two-echo SPGR tagged cardiac images acquired through systole. Six of 12 time frames are shown, each with 18-ms time resolution, acquired in 12 heartbeats. Two full echoes were used in this acquisition, with TR = 4.5 msec, TE = 1.6 msec, 24-cm FOV, 8-mm slice thickness, BW = ± 64 kHz, 128 \times 120 matrix size, 10° flip angle, and eight phase-encoding lines per image per heartbeat. No post-processing corrections were made for this acquisition.

Images acquired with fractional echoes (one, two, and three echoes) showed minimal blurring and image quality and SNR comparable to the full echo images (images not shown). A minimal difference was observed between images acquired with and without fractional echoes (data not shown). Increasing echo train length to two fractional echoes from a single full echo decreases total imaging time by 48%.

In Vivo Cardiac Images

Figure 9 shows a cine sequence of tagged cardiac images from a human volunteer, acquired through systole using a two-echo sequence. Image parameters include TR = 4.5 msec, TE = 1.6 msec, 24-cm FOV, 8-mm slice thickness, 128 \times 120 data matrix (full echo), 10° tip angle, and eight phase-encoding lines per image per heartbeat. Image quality of the two-echo acquisition was comparable to single-echo images, as seen in Fig. 10. This figure shows a midsystolic single-echo image and the two-echo image acquired at the same time point in systole. Centric phase encoding (29) was used for both acquisitions. The SNR of end-systolic images of both acquisitions was 19. Although the images have comparable image quality, the two-echo acquisition required 30% fewer heartbeats. If this additional time were to be used for averaging, the SNR of the two-echo images would be 14% higher, reflecting the 30% efficiency increase afforded by increasing the echo train length from one to two.

Perfusion experiments were performed in the canine heart with a two-echo sequence with a saturation recovery technique using nonselective saturation with reverse centric phase encoding, as described by Boxerman et al. (29). Peripheral venous bolus injection of Gd-DTPA (2.5 ml) was tracked by imaging three short-axis slices every heartbeat, as shown in Fig. 11. Nonselective presaturation, followed by reverse centric phase encoding, provided excellent enhancement of the right and left ventricular blood pools as well as the myocardium. Imaging parameters included a 28-cm FOV, 10-mm slice thickness, 20° flip angle, ± 64 -kHz bandwidth, $N_x = 160$ (full echo), and $N_y = 72$.

The average time per echo of the two-echo acquisition was 2.4 msec, requiring a total of 176 msec to acquire a single image, including time for presaturation pulses. With the dog's heart rate of 90 bpm, this allowed collection of three slices. The equivalent single-echo sequence (TR = 3.4

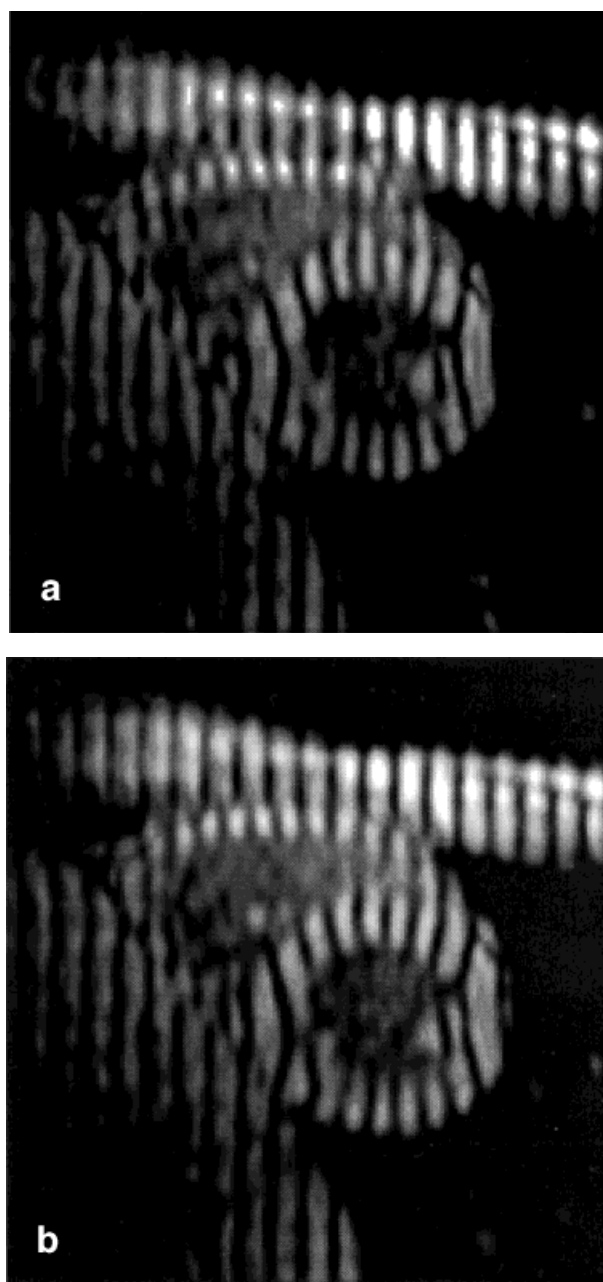


FIG. 10. Midsystolic single-echo tagged cardiac image with $TR = 3.2$ msec and $TE = 1.6$ msec (a) and two-echo image acquired at the same time point, with $TR = 4.5$ msec and $TE = 1.6$ msec (b). Other imaging parameters include a 24-cm FOV, 8-mm slice thickness, $BW = \pm 64$ kHz, 128×120 matrix size, and 10° flip angle. Six phase-encoding lines per image per heartbeat were acquired for single-echo images; this was increased to eight for the two-echo acquisition while maintaining the same time resolution (18 msec). This represents a 33% reduction in scan time while maintaining comparable image quality. Centric phase encoding was used for both acquisitions.

msec) required 248 msec per image and was able to acquire a maximum of two slices per heartbeat (data not shown). At a heart rate of 65 bpm, the two-echo sequence could acquire five slices per heartbeat with the same imaging parameters, while the single-echo sequence could acquire three.

DISCUSSION

An ultrafast multi-echo SPGR sequence with HOT optimization was described and its speed and efficiency performance investigated. HOT pulses were used to achieve the shortest possible dead times and highest efficiency possible for a given set of imaging parameters. It was shown that significant incremental improvements in the speed performance and efficiency of the sequence could be achieved by adding even small numbers of echoes to the echo train. The efficiency of this sequence is slightly higher than cardiac spiral MRI (7, 30), where sequence efficiencies typically range from 50% to 55% (AB Kerr, personal communication).

It was also shown that speed and efficiency performance will not increase significantly by improving gradient hardware performance. This has been previously demonstrated for single-echo sequences (12). Improvement in speed performance is best achieved by increases in receiver bandwidth, but at a cost of reduced SNR. The use of higher bandwidths will require the use of high maximum gradient strengths, however.

Expressions for choosing the optimal echo train length were derived. For steady-state imaging, it was shown that the optimal echo train duration is approximately T_2^* . For conditions where the steady state has not been reached, the optimal echo train duration is less than T_2^* . Owing to focal regions of inhomogeneity, the minimum T_2^* found in the myocardium is approximately 12 msec (14); this means that the maximum echo train duration for cardiac imaging is 12 msec.

A theoretical description of the PSF for a two-echo sequence was presented under Ghosting with Small Echo Train Lengths, and it was found that phase discontinuities cause blurring artifacts, rather than ghosting. This implies that short echo train sequences can avoid the use of chemical presaturation pulses used to null the signal from fat. Furthermore, echo time shifting, which is often used to smooth phase and amplitude discontinuities in the phase-encoding direction of k-space, can be avoided. This is important for low echo train length sequences, since echo time shifting greatly reduces the speed and efficiency performance of these sequences. This analysis also implies that precise correction of timing delays and phase offsets from hardware inaccuracies are not required; this greatly simplifies image reconstruction. The quality of low echo train images in phantoms and in vivo was excellent, and, as expected, images exhibited minimal blurring while achieving 20% to 48% decreases in total imaging time.

Fractional echoes are highly effective at reducing imaging time while maintaining image resolution. Sequence efficiency, and hence SNR, will suffer with fractional readout, although little change in image quality was observed. For our scanner, a two-echo sequence with fractional echoes has speed performance superior to a 10-echo train length sequence with full echoes.

Criteria for establishing maximum echo train lengths for reduction of image distortion were also described. For field inhomogeneities experienced in the heart (14), no more than two to three echo train lengths should be used to maintain distortion less than 0.5 pixels. Chemical shift artifact reduction for EPI sequences with long echo trains often requires the application of spatial spectral excitation (31). For short echo train length sequences, the additional

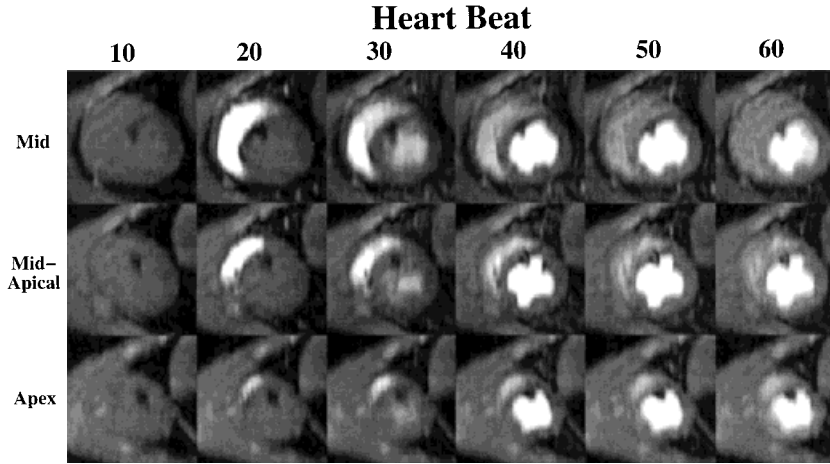


FIG. 11. Two-echo short-axis saturation recovery images in three slices of a canine heart, acquired every heartbeat to track the passage of a peripheral bolus injection of Gd-DTPA. The heart rate was 90 bpm, and the total time required for each image was 176 msec, with $N_x = 160$ (full echo), $N_y = 72$, 28-cm FOV, 10-mm slice thickness, and ± 64 -kHz bandwidth. Nonselective presaturation with reverse centric phase-encoding and a 20° flip angle were used to maximize T_1 contrast. The black void in the LV is a pigtail catheter not used for this experiment.

overhead of spatial spectral pulses (approximately 15 msec on our scanner) completely rules out the use of such pulses. The improved speed performance of this sequence allows echoes to be acquired every 2.2 msec, on average, depending on the imaging parameters. This increase in imaging speed can be applied to a variety of cardiac imaging applications.

For example, perfusion studies that track the arrival of contrast agents after bolus injection will benefit from higher temporal resolution and an increased number of image planes. In this work, a saturation recovery technique with reverse centric phase encoding (29) was used in conjunction with a two-echo sequence to acquire three slices (160×72) every heartbeat in a canine model with a heart rate of 90 bpm. The equivalent single-echo sequence was capable of acquiring only two slices during this RR interval. At slower heart rates, typical of humans, up to five slices could be imaged every heartbeat, with 72–80 phase-encoding lines per image. The increase in the number of imaging planes has been made possible through the addition of one echo to the echo train.

Another important application of rapid cardiac imaging is human stress testing during dobutamine infusion, which requires acquisition of movies from a minimum of seven to nine imaging planes in one to three breath-holds. This implies that a movie from a single imaging plane must be acquired in approximately three heartbeats. The multi-echo sequence presented in this article can achieve this goal if each image has 66 phase-encoding lines and a 50-msec time resolution.

For continuous “fluoroscopic” monitoring (6), this sequence will allow complete image updates with a refresh rate of 8 Hz for images with 60 phase-encoding steps, ± 64 -kHz bandwidth, a 2.2 G/cm maximum gradient strength, and a 120 T/m s slew rate. Increases in bandwidth and hardware performance, as seen in Fig. 6a,c, will increase this refresh rate to approximately 12 Hz. In conclusion, the addition of one to two echoes to standard SPGR sequences can make significant improvements in speed and efficiency performance for cardiac imaging while maintaining good image quality, without the need for chemical presaturation, reference scans, or special post-processing reconstruction computations.

ACKNOWLEDGMENTS

This research was supported by NIH grant HL45683 and a Whitaker Foundation Biomedical Research Grant. SBR is

supported with a Medical Scientist Training Program (MSTP) Fellowship. ERM is an Established Investigator of the American Heart Association.

APPENDIX A

Optimization of Echo Train Length

Differentiation of Eq. 8 with respect to the echo train length, n , and setting the result to zero,

$$\frac{dS}{dn} = \frac{d}{dn} \left(\frac{(1 - e^{-T_d/T_1} e^{-nT_{ro}/T_1}) e^{-n\zeta T_{ro}/T_2^*}}{\sqrt{1 - e^{-2T_d/T_1} e^{-2nT_{ro}/T_1}}} \right) = 0 \quad [14]$$

Performing the differentiation and simplifying,

$$\frac{\zeta T_1}{T_2^*} (e^{-T_d/T_1} e^{-nT_{ro}/T_1})^2 + e^{-T_d/T_1} e^{-nT_{ro}/T_1} - \frac{\zeta T_1}{T_2^*} = 0 \quad [15]$$

Applying the quadratic equation,

$$e^{-T_d/T_1} e^{-nT_{ro}/T_1} = -\frac{T_2^*}{2\zeta T_1} \pm \sqrt{1 + \left(\frac{T_2^*}{2\zeta T_1}\right)^2} \quad [16]$$

Choosing the positive solution and solving for the optimal echo train length,

$$n_{opt} = -\frac{T_d}{T_1} - \frac{T_1}{T_{ro}} \ln \left(\sqrt{1 + \left(\frac{T_2^*}{2\zeta T_1}\right)^2} - \frac{T_2^*}{2\zeta T_1} \right) \quad [17]$$

If $T_2^*/2\zeta T_1 \ll 1$, then Eq. 17 can be expanded as a Taylor series and simplified to

$$n_{opt} = \frac{T_2^*}{2\zeta T_{ro}} - \frac{T_d}{T_1} \approx \frac{T_2^*}{2\zeta T_{ro}} \quad [18]$$

APPENDIX B

Distortion in the Phase-Encoding Direction

For an interleaved EPI acquisition with N_y phase-encoding steps, n_i interleaves (N_y/n), and echo train shifting (32), the additional phase of even (+) or odd (−) echoes caused by

off-resonance effects is

$$\phi_{\pm}(k_x, n_y \Delta k_y) = \left(\Delta B(x, y) + \frac{2\pi f}{\gamma} \right) \left(\pm \frac{k_x}{G_x} + \frac{T_{ro}}{\Delta G_y \Delta t_y n_i} n_y \Delta k_y \right) \quad [19]$$

where n_y is the phase-encoding index ($n_y = -N_y/2, \dots, N_y/2 - 1$ for spin echo EPI, and $N_y = 0, \dots, N_y - 1$ for gradient echo EPI), $\Delta k_y = \gamma \Delta G_y \Delta t_y n_i$ is the blip size in the phase-encoding direction, G_x is the magnitude of the readout gradient, and k_x is the k position in the readout direction, rastering in two directions (\pm) for even (+) and odd (−) echoes. The total signal from the object is then

$$s_{\pm}(k_x, n_y \Delta k_y) = \sum_l \int \int \rho_l(x, y) e^{j k_x (x \pm \Delta B(x, y) + 2\pi f_l / \gamma) / G_x} e^{j n_y \Delta k_y (y + t_{ro}(\Delta B(x, y) + 2\pi f_l / \gamma) / n_i \Delta G_y \Delta t_y)} dx dy \quad [20]$$

where $\rho_l(x, y)$ is the density of protons in chemical species l , having an off-resonance shift of f_l . The first exponential term in the integrand reveals a distortion in the x -direction due to inhomogeneities and chemical shift. In practice, however, the readout gradient is sufficiently strong to make this effect small, and, for this reason, this distortion will be ignored.

The second exponential term, however, describes a substantial distortion in the phase-encoding direction, since the time between readout gradients is significant and the area under a phase-encoding gradient is small. Increasing the number of interleaves reduces distortion and the effects of chemical shift, as will reducing the time between readout gradients. This distortion, Δy (cm), is written

$$\Delta y = \frac{T_{ro}(\Delta B(x, y) + f_l / \gamma)}{n_i \Delta G_y \Delta t_y} \quad [21]$$

This is similar to expressions for distortion previously reported (11, 17). Alternatively, the shift can be expressed in pixels, noting that $\Delta k_y = 2\pi / FOV$, $\Delta y' = \Delta y N_y / FOV$, and $n = N_y / n_i$,

$$\begin{aligned} \Delta y' &= \frac{\gamma}{2\pi} (\Delta B(x, y) + f_l / \gamma) T_{ro} n \\ &= \frac{\gamma}{2\pi} (\Delta B(x, y) + f_l / \gamma) T_{smp} \end{aligned} \quad [22]$$

where the total sampling time of an echo train is $T_{smp} = T_{ro} n$.

REFERENCES

- Atkinson DJ, Burstein D, Edelman RR. First-pass cardiac perfusion: evaluation with ultrafast MR imaging. *Radiology* 1990;174:757–762.
- Moseley ME, Sevik R, Wendland MF, et al. Ultrafast magnetic resonance imaging: diffusion and perfusion. *Can Assoc Radiol J* 1991;42:31–38.
- Wendland MF, Saeed M, Masui T, Derugin N, Moseley ME, Higgins CB. Echo-planar MR imaging of normal and ischemic myocardium with gadodiamide injection. *Radiology* 1993;186:535–542.

- Edelman RR, Li W. Contrast-enhanced echo-planar MR imaging of myocardial perfusion: preliminary study in humans. *Radiology* 1994;190:771–777.
- Schwittner J, Debatin JF, von Schulthess GK, McKinnon GC. Normal myocardial perfusion assessed with multishot echo-planar imaging. *Magn Reson Med* 1997;37:140–147.
- Riederer SJ, Tasciyan T, Farzaneh F, Lee JN, Wright RC, Herfkens RJ. MR fluoroscopy: technical feasibility. *Magn Reson Med* 1988;8:1–15.
- Kerr AB, Pauly JM, Meyer CH, Nishimura DG. New strategies in spiral MR fluoroscopy. In: *Proceedings, ISMRM, Third Annual Meeting, Nice, France, 1995*. p. 99.
- Mansfield P. Multi-planar image formation using NMR spin-echoes. *J Phys Chem* 1977;10:L55–L58.
- Hennig J, Nauerth A, Friedburg H. RARE imaging: a fast imaging method for clinical MR. *Magn Reson Med* 1986;3:823–833.
- Oshio K, Feinberg DA. GRASE (Gradient- and spin-echo) imaging: a novel fast MRI technique. *Magn Reson Med* 1991;20:344–349.
- McKinnon GC. Ultrafast interleaved gradient-echo-planar imaging on a standard scanner. *Magn Reson Med* 1993;30:606–616.
- Reeder SB, McVeigh ER. The effect of high performance gradients on fast gradient echo imaging. *Magn Reson Med* 1994;32:612–621.
- Tang C, McVeigh ER, Zerhouni EA. Multi-shot EPI for improvement of myocardial tag contrast: comparison with segmented SPGR. *Magn Reson Med* 1995;33:443–447.
- Reeder SB, Faranesh AZ, Boxerman JL, McVeigh ER. In vivo measurement of T2* and field inhomogeneity maps in the human heart at 1.5 T. *Magn Reson Med* 1998;39:988–998.
- Atalar E, McVeigh ER. Minimization of dead-periods in MRI pulse sequences for imaging oblique planes. *Magn Reson Med* 1994;32:773–777.
- Duerk JL, Simonetti OP. Theoretical aspects of motion sensitivity and compensation in echo-planar imaging. *J Magn Reson Imaging* 1991;1:643–650.
- Farzaneh F, Riederer SJ, Pelc NJ. Analysis of T2 limitations and off-resonance effects on spatial resolution and artifacts in echo-planar imaging. *Magn Reson Med* 1990;14:123–139.
- McVeigh ER. MRI of myocardial function: motion tracking techniques (Review). *Magn Reson Imaging* 1996;14:137–150.
- Feinberg DA, Oshio K. Gradient echo shifting in fast MRI techniques (GRASE imaging) for correction of field inhomogeneity errors and chemical shift. *J Magn Reson* 1992;97:177–183.
- Reeder SB, Atalar E, Bolster BDI, McVeigh ER. Quantification and reduction of ghosting artifacts in interleaved echo-planar imaging. *Magn Reson Med* 1997;38:429–439.
- Bruder H, Fischer H, Reinfelder HE, Schmitt F. Image reconstruction for echo planar imaging with nonequidistant k-space sampling. *Magn Reson Med* 1992;23:311–323.
- McVeigh ER, Gao L. Precision of tag position estimation in breath-hold cine MRI: the effect of tag spacing. In: *Proceedings of the SMRM, Twelfth Annual Meeting, New York, 1993*. p. 199.
- Mosher TJ, Smith MB. A DANTE tagging sequence for the evaluation of translational sample motion. *Magn Reson Med* 1990;15:334–339.
- Axel L, Dougherty L. MR imaging of motion with spatial modulation of magnetization. *Radiology* 1989;171:841–845.
- Croisille P, Guttman MA, Atalar E, McVeigh ER, Zerhouni EA. Precision of myocardial contour estimation from tagged MR images with a “black-blood” technique. *Acad Radiol* 1998;5:93–100.
- Wang Y, Grimm RC, Rossman PJ, Debbins JP, Riederer SJ, Ehman RL. 3D coronary MR angiography in multiple breath-holds using a respiratory feedback monitor. *Magn Reson Med* 1995;34:11–16.
- McVeigh ER, Atalar E. Cardiac tagging with breath-hold cine MRI. *Magn Reson Med* 1992;28:318–327.
- Faranesh AZ, Reeder SB, McVeigh ER. “Compensation blips” for referenceless EPI. In: *Proceedings of the ISMRM, Sixth Annual Meeting, Sydney, Australia, 1998*. p. 420.
- Boxerman JL, Reeder SB, Zerhouni EA. Standard vs. centric segmented k-space phase encoding: SNR comparison in breath-hold SPGR cardiac imaging. In: *Proceedings of the ISMRM, Fifth Annual Meeting, Vancouver, B.C., Canada, 1997*. p. 138.
- Meyer CH, Hu BS, Nishimura DG, Macovski A. Fast spiral coronary artery imaging. *Magn Reson Med* 1992;28:202–213.
- Meyer CH, Pauly JM, Macovski A, Nishimura DG. Simultaneous spatial and spectral selective excitation. *Magn Reson Med* 1990;15:287–304.
- Feinberg DA, Oshio K. Phase errors in multi-shot echo planar imaging. *Magn Reson Med* 1994;32:535–539.